Supporting Information

Heterointerface MnO_2/RuO_2 with rich oxygen vacancies for enhanced oxygen evolution in acidic media

Zhiming Guan, Qian Chen, Lin Liu, Chenghui Xia*[a], Lixin Cao*[a], Bohua Dong*[a]

[a]School of Materials Science and Engineering, Ocean University of China, No. 1299, Sansha Road, Huangdao District, Qingdao, 266000, People's Republic of China.

*Corresponding Author

Bohua Dong, E-mail: dongbohua@ouc.edu.cn

Lixin Cao, E-mail: caolixin@ouc.edu.cn

Chenghui Xia，E-mail: c.xia@ouc.edu.cn

This PDF file includes:

Supporting Information Text

Figures S1 to S14

Tables S1 to S4

SI References

Supporting Information Text

1. Experimental Section

1.1 Materials

Manganese (II) chloride ($MnCl_2$, >99 %), Ammonium bicarbonate (NH_4HCO_3, >99.5 %), Potassium permanganate ($KMnO_4$, >98 %), Ruthenium (III) chloride hydrate ($RuCl_3 \cdot xH_2O$, 35.0-42.0 %), Hydrochloric acid (HCl, 37 %) and Sulfuric acid (H_2SO_4, 97 %) were purchased from Aladdin. Deionized water (resistivity >18 MΩ·cm) used throughout the experiment was purified by the GWA-UN1-F20 system (Beijing Purkinje General Instrument Co., Ltd). Ethanol was purchased from Beijing Tongguang Fine Chemicals Co., Ltd. Carbon cloth (CC) was purchased from Shanghai Hesen Electric Co., Ltd. Alfa Aesar supplied Nafion solution (5 wt.%). All chemicals were used without further purification.

1.2 Synthesis of MnO_2/RuO_2

Dissolve 1 mmol of $MnCl_2$ in 50 ml of deionized water and stir thoroughly. Dissolve 10 mmol of NH_4HCO_3 in a mixture of 55 ml of anhydrous ethanol and deionized water (V_{water}: $V_{ethanol}$ = 10:1) and stir the mixture well. After combining the two solutions and stirring at 60 ℃ in a water bath, the colorless solution will turn milky white, indicating the formation of $MnCO_3$. Once the reaction is complete, collect the white precipitate by centrifugation and wash it multiple times with deionized water. Mix the obtained white precipitate of $MnCO_3$ with 40 ml of deionized water and stir thoroughly. Add 5 ml of the 0.03 $mol \cdot L^{-1}$ $KMnO_4$ solution and stir for 0.5 h. Then add 5 ml of a 5 $mol \cdot L^{-1}$ hydrochloric acid solution and stir for an additional 0.5 h. Collect the brown precipitate by centrifugation and wash it multiple times with deionized water. Mix the precipitate with 60 ml of deionized water and stir evenly. Add X mmol of $RuCl_3 \cdot xH_2O$ and stir vigorously for 6h. Collect the black precipitate by centrifugation and wash it multiple times with deionized water. Dry the precipitate in a vacuum oven at 60 ℃ overnight to obtain a powdery product. The resulting powdery product is first sintered in N_2 at 350 ℃ for 2 h, then sintered in air at 350 ℃ for an additional 2 h. The product obtained is named $MnO_2/XRuO_2$, (X = 0.10, 0.15, 0.20), $MnO_2/0.15RuO_2$ is abbreviated as MnO_2/RuO_2. For samples with different Ru contents, the synthesis process remains the same in all steps except for the Ru addition. For samples with 0.1 mmol of $RuCl_3 \cdot xH_2O$, 0.15 mmol of $RuCl_3 \cdot xH_2O$ and 0.2 mmol of $RuCl_3 \cdot xH_2O$, respectively. Samples without the addition of $RuCl_3 \cdot xH_2O$ are named MnO_2.

1.3 Electrode preparation

5.0 mg of catalyst was dispersed in a mixture of 740 μl of anhydrous ethanol, 240 μl of deionized water, and 20 μl of Nafion (5 wt.%), and ultrasonically dispersed for 1 h to obtain a homogeneously dispersed ink, and then 200 μl of ink was drop-coated onto a 1 x 1 cm^2 carbon cloth (CC) with a catalyst loading of 1 $mg \cdot cm^{-2}$. After drying at room temperature, the electrochemical tests can be performed.

2. Electrochemical measurements of the OER

All electrochemical tests were obtained using a CHI760E electrochemical workstation (ChenHua Instruments, Shanghai, China) with a standard three-electrode system at room temperature. The working electrode (working area of 1 × 1 cm^2) was a carbon cloth loaded with catalyst, and carbon rods and Ag/AgCl (saturated KCl) were used as counter electrodes and reference electrodes, respectively. A commercial RuO_2 (RuO_2) catalyst with the same loading amount was used as the reference catalyst. Prior to testing, the electrocatalyst was subjected to cyclic voltammetry (CV) activation of the electrodes in the voltage range of 1.0-1.4 V vs. Ag/AgCl until a stable CV curve was obtained before testing. Linear scanning voltammetry (LSV) was performed at a scan rate of 5 $mV \cdot s^{-1}$. Electrochemical impedance spectroscopy (EIS) measurements were performed in a 0.5 M H_2SO_4 solution at an open-circuit voltage vs. RHE in the frequency range of 10 kHz to 0.1 Hz. The results were presented in the form of Nyquist plots and fitted to representative equivalent circuits using the ZView software. The electrochemical double layer capacitance (C_{dl}) was calculated by analyzing the CV curves at different scan rates of 10, 20, 40, 60, 80, and 100 $mV \cdot s^{-1}$. A total of 10000 CV cycles and chronopotential tests were performed to evaluate the durability of the electrochemical catalysts. All potentials measured in a 0.5 M H_2SO_4 electrolyte were converted to reversible hydrogen electrodes (RHE) via the Nernst equation (1):

$$E_{RHR} = E_{Ag/AgCl} + 0.0591 \times pH + 0.197 \quad (1)$$

Due to the resistance between the catalyst and electrolyte interface, the polarization curves were corrected for 90% compensation based on the iR in the electrolyte. The Tafel slope is calculated from the Tafel equation (2):

$$\eta = b \times \log j + a \quad (2)$$

where η is the overpotential, b is the Tafel slope, j is the current density, and a is a constant.

2.1 Calculation of the mass activity

The mass activity (j $A \cdot g^{-1}_{Ru}$) of MnO_2/RuO_2 and RuO_2 catalysts was determined using equation (3):

$$j\ (A \cdot g_{Ru}^{-1}) = \frac{j_{geo} \times A_{geo}}{m_{Ru}} \quad (3)$$

where m_{Ru} is the mass of Ru loaded on the carbon cloth calculated from the ICP-OES analysis, A_{geo} is the geometric area, and j_{geo} is the geometric current density.

2.2 Calculation of TOF

The TOF of MnO_2/RuO_2 and RuO_2 catalysts was determined using equation (4):

$$\begin{aligned} \text{TOF}\ (O_2\ h^{-1}) &= 3600 \times \text{TOF}\ (O_2\ s^{-1}) \\ &= 3600 \times \frac{O_2 \text{ turnovers per } A_{geo}}{\text{Active sites per } A_{geo}} \end{aligned} \quad (4)$$

From the geometric current density of the LSV polarization curve, the O_2 conversion rate per geometric area can be derived. is derived from the geometric current density of the LSV polarization curve according to equation (5):

$$\begin{aligned} &O_2 \text{ turnovers per } A_{geo} \\ &= j_{geo} \times \frac{1C \cdot s^{-1}}{1000mA} \times \frac{1mol}{96485.3C} \times \frac{1}{4} \times \frac{6.023 \times 10^{23}}{1\ mol\ O_2} \end{aligned} \quad (5)$$

It is assumed that all the Ru atoms in the catalyst are active sites. Therefore, the number of active sites per geometrical area is equal to the number of Ru atoms per geometrical area, which can be calculated from the results of the ICP-OES analysis.

2.3 Characterizations

X-ray diffraction (XRD) tests were conducted using a Bruker D8 Advance X-ray diffractometer equipped with a copper target and a scanning speed of 5 °/min. Scanning electron microscopy (SEM) measurements were carried out on a Gemini300 field scanning electron microscope operating at an accelerating voltage of 5 kV. High-resolution transmission electron microscopy (HRTEM) images were obtained using a JEOL JEM-F200 instrument with an accelerating voltage of 200 kV, coupled with the JED-2300T spectroscopy model. The X-ray photoelectron spectroscopy (XPS) spectra of the samples were acquired using a Thermo Scientific K-Alpha photoelectron spectrometer. The obtained XPS spectra were charge-corrected and adjusted using a C 1s line at 284.8 eV, followed by curve fitting analysis. Electron paramagnetic resonance spectroscopy (EPR) was obtained by testing on a Bruker EMX PLUS, Germany. Inductively Coupled Plasma Optical Emission Spectroscopy (ICP-OES) analysis was performed on an Agilent 5110 instrument.

Supporting Figures

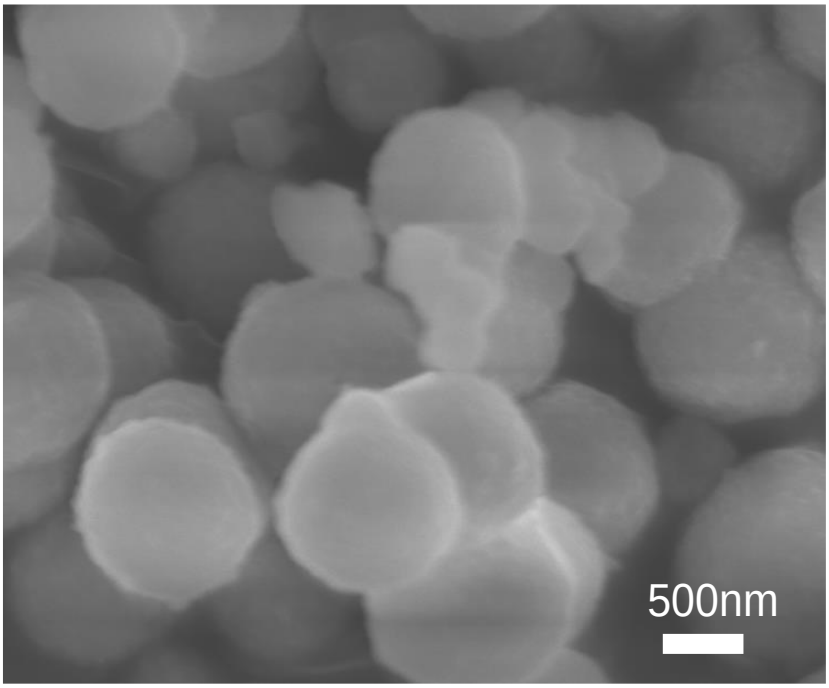

Fig. S1. SEM image of $MnCO_3$.

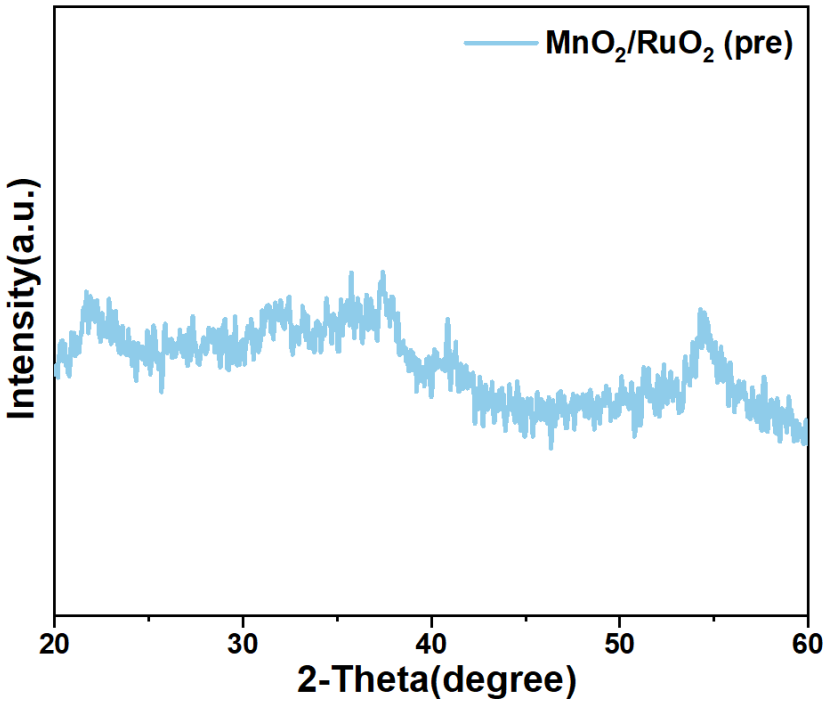

Fig. S2. XRD pattern of precursor MnO_2/RuO_2(pre).

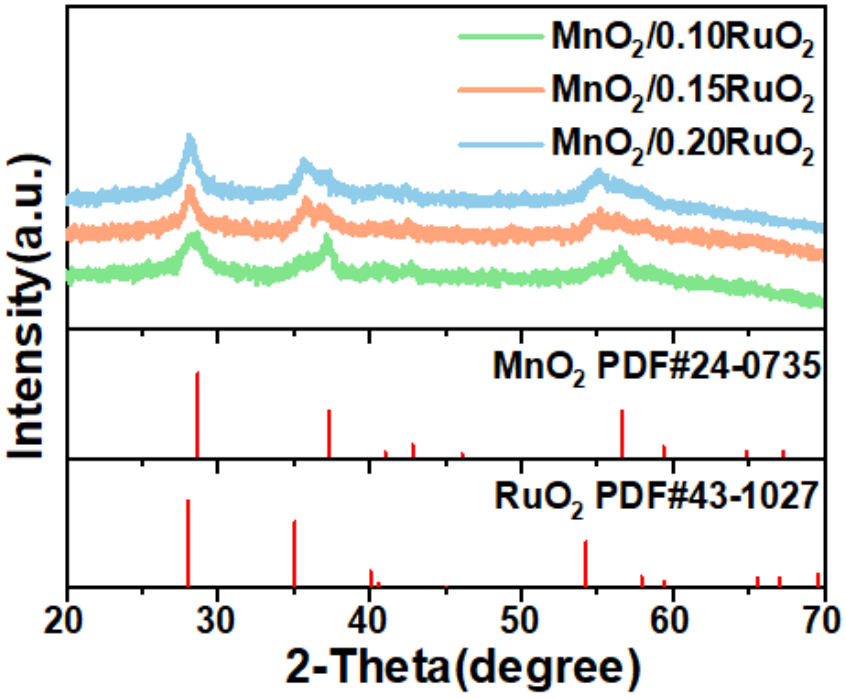

Fig. S3. XRD patterns of $MnO_2/0.10RuO_2$, $MnO_2/0.15RuO_2$ and $MnO_2/0.20RuO_2$.

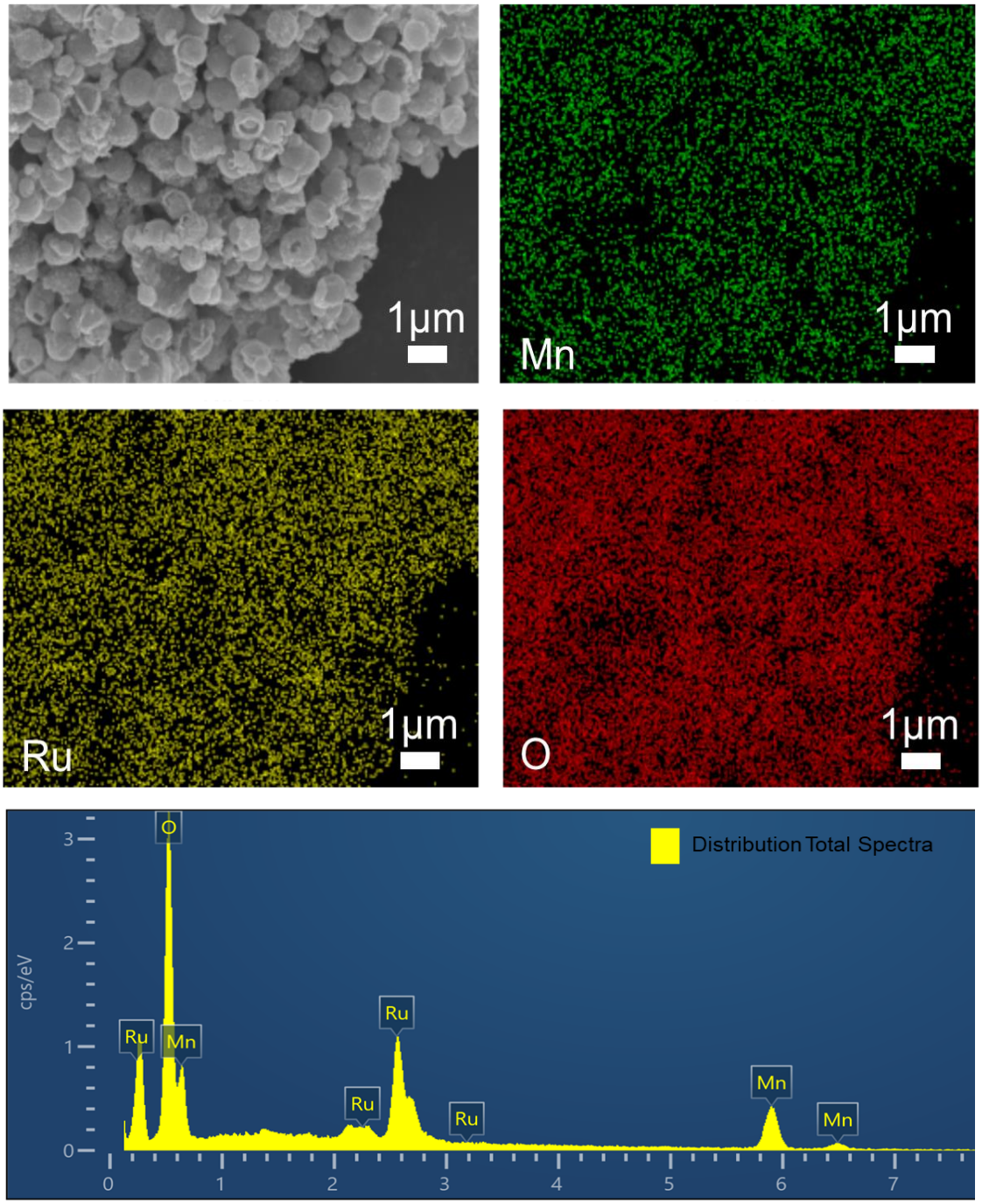

Fig. S4. EDX elemental mapping images of MnO_2/RuO_2, including the Mn, Ru, and O elements.

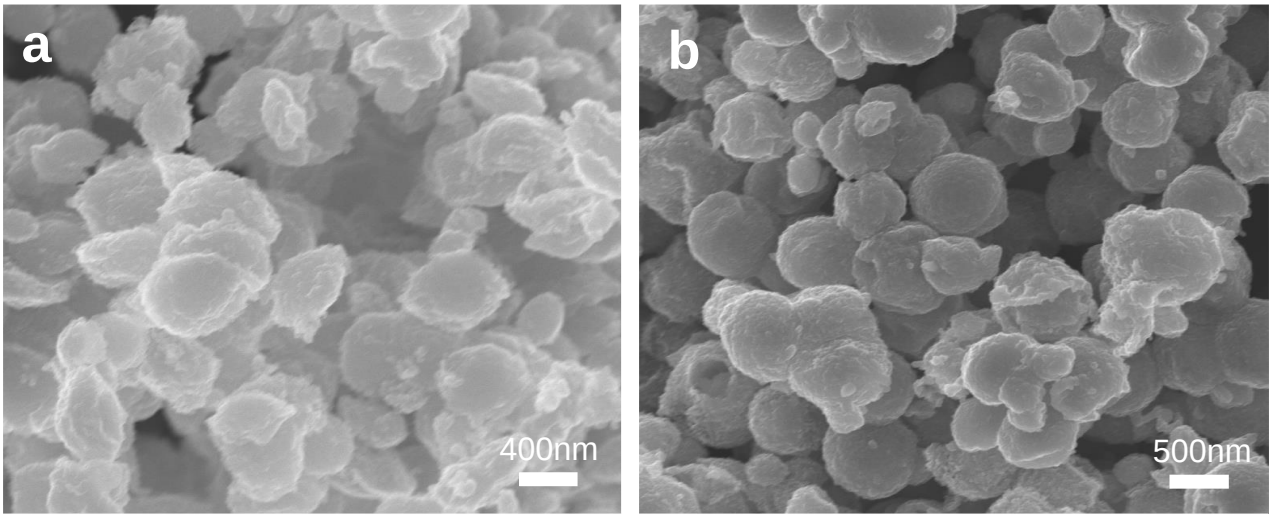

Fig. S5. SEM image of MnO_2/0.10RuO_2 (a) and MnO_2/0.20RuO_2 (b).

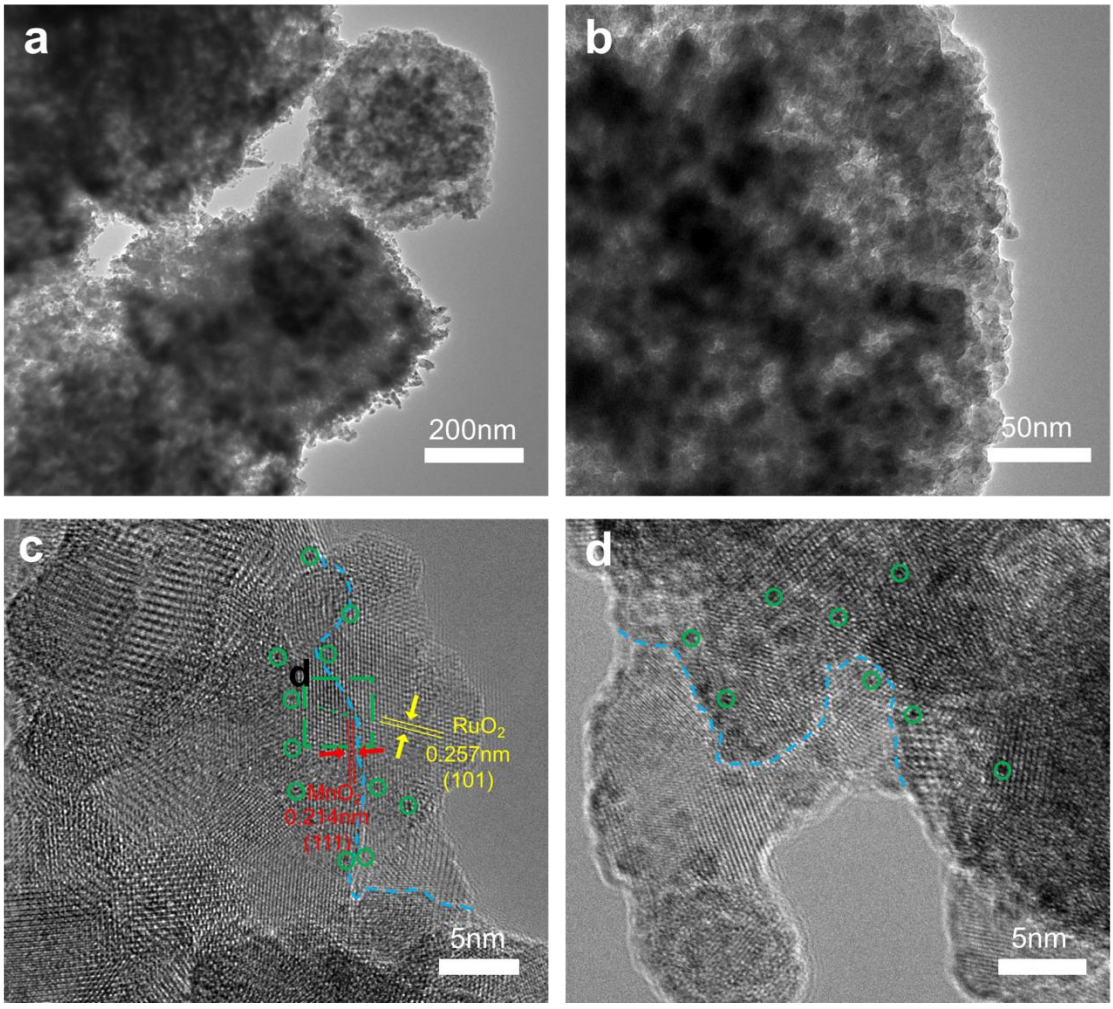

Fig. S6. (a-d) HRTEM image of MnO_2/RuO_2.

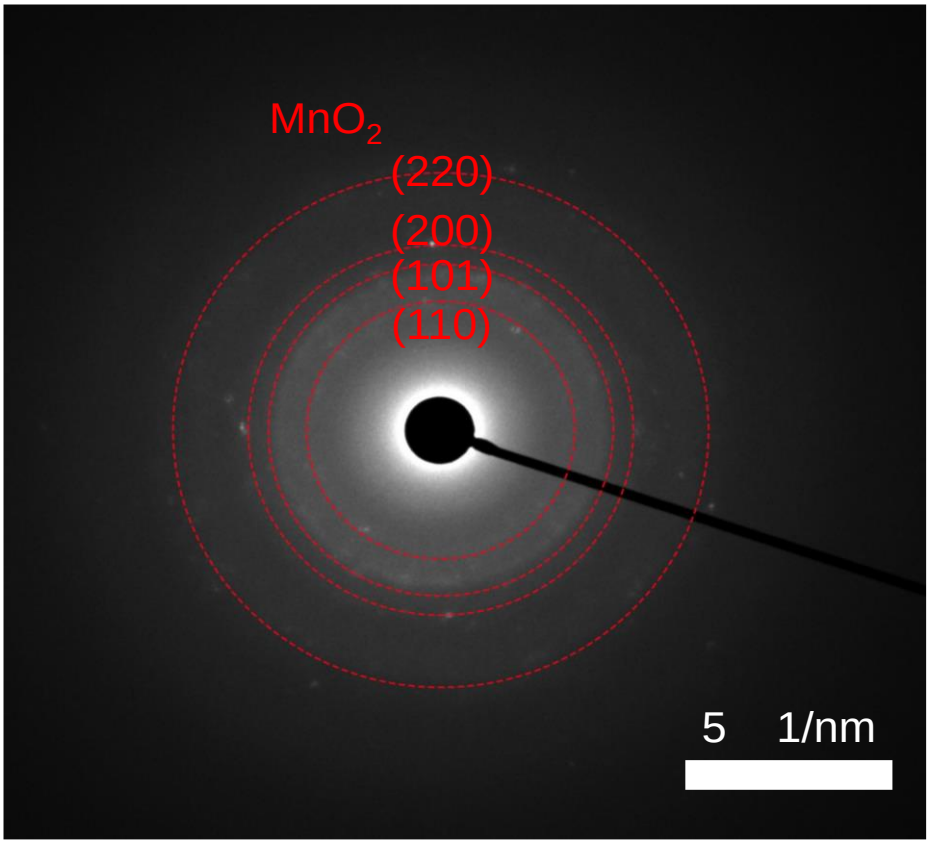

Fig. S7. The corresponding selected area electron diffraction for MnO_2/RuO_2.

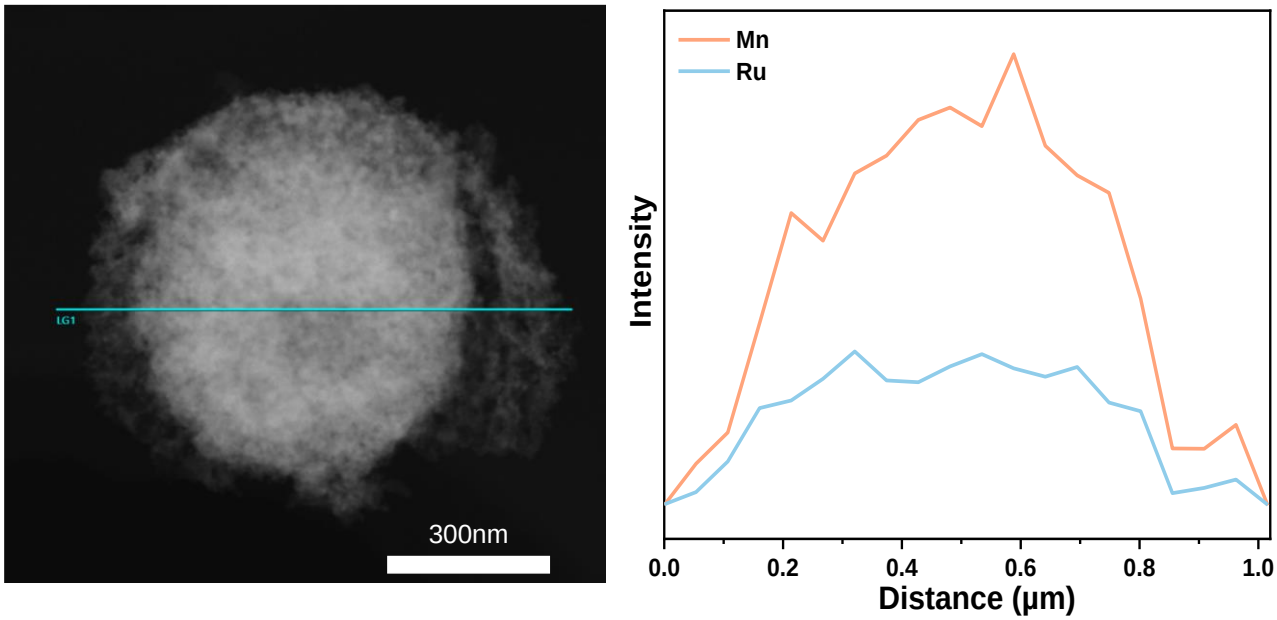

Fig. S8. EDS line-scan profile along the grey line in the HRTEM image and corresponding simulation curves.

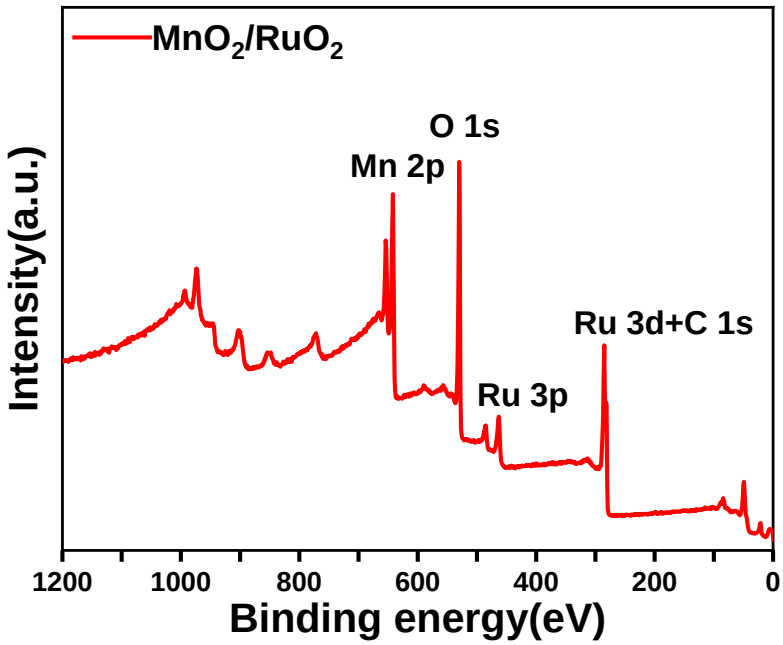

Fig. S9. XPS survey spectrum of MnO_2/RuO_2.

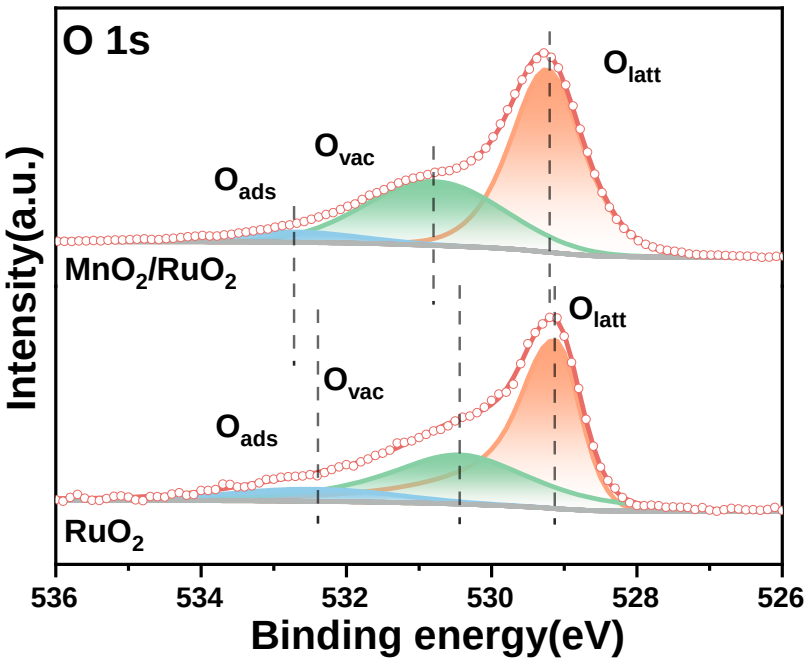

Fig. S10. High-resolution XPS spectra of O 1s for MnO_2/RuO_2 and RuO_2.

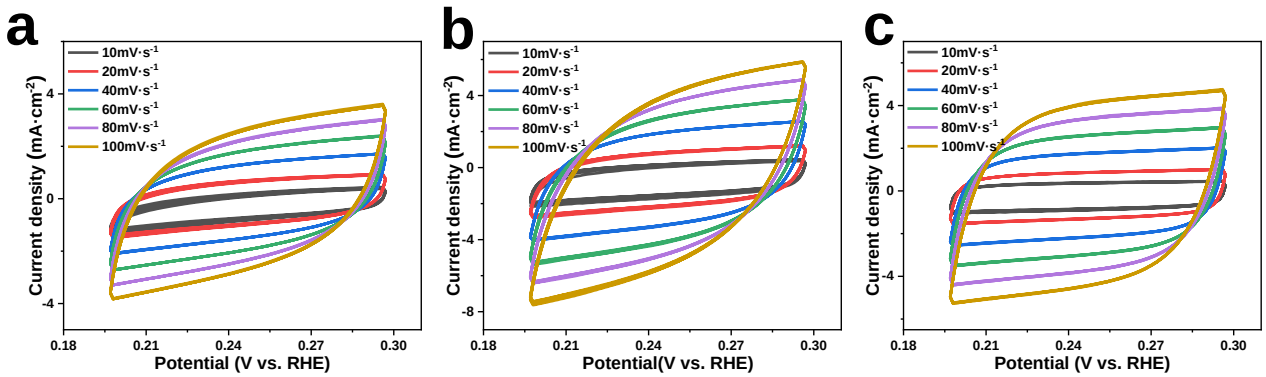

Fig. S11. The CV curves of $MnO_2/0.10RuO_2$ (a), $MnO_2/0.15RuO_2$ (b) and $MnO_2/0.20RuO_2$ (c) with the scan rate ranging from 10 to 100 $mV \cdot s^{-1}$ in 0.5 M H_2SO_4, the C_{dl} values at the potential of 0.247 V.

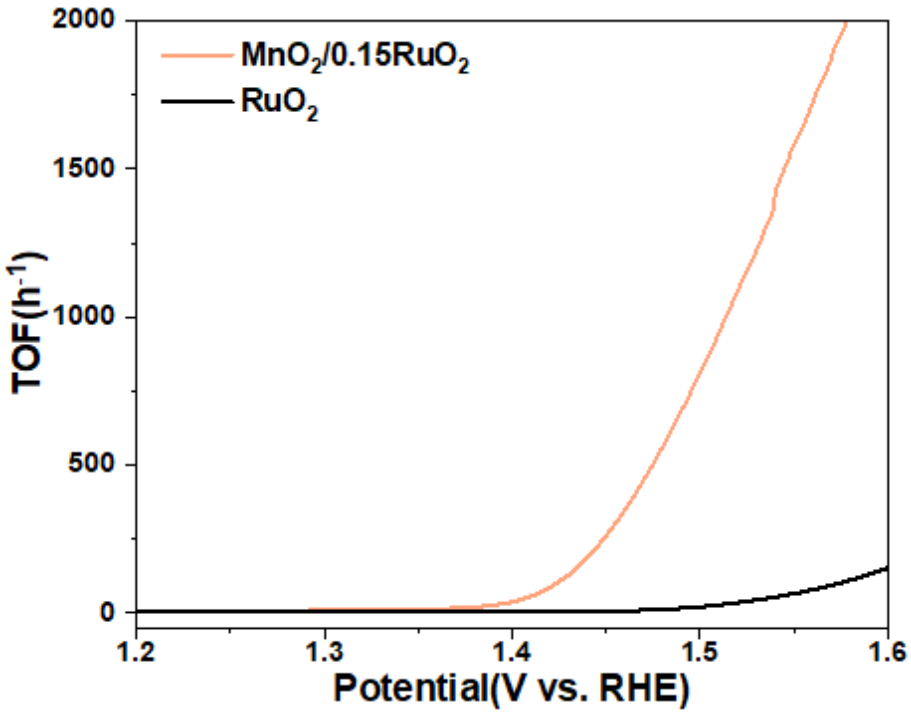

Fig. S12. TOF of MnO_2/RuO_2 and RuO_2 electrode.

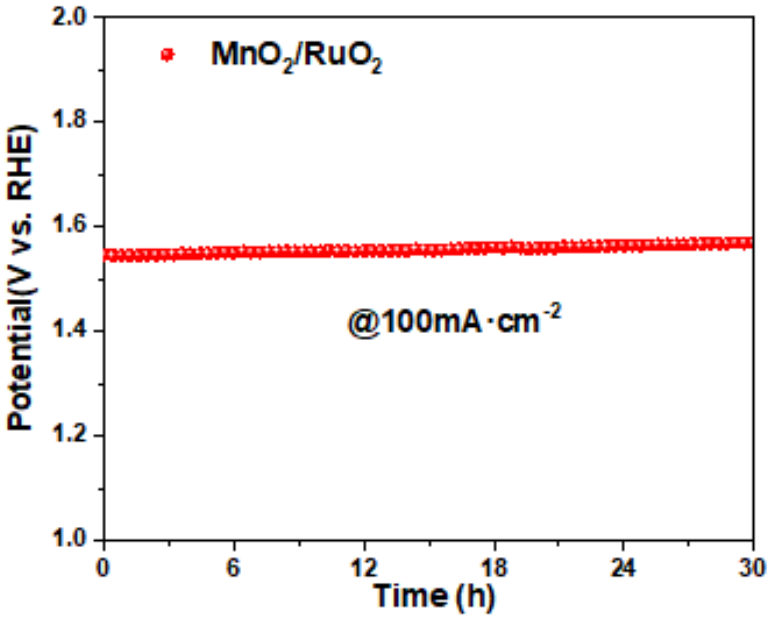

Fig. S13. Chronopotentiometry measurement without iR compensation at the OER current density of 100 mA·cm^{-2} for MnO_2/RuO_2 electrode.

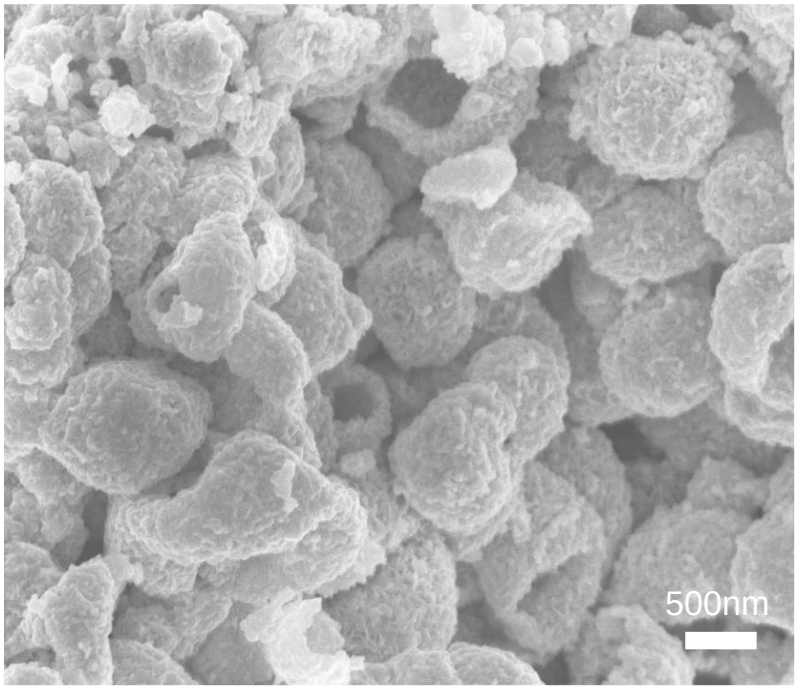

Fig. S14. (a) SEM image of MnO_2/RuO_2 sample after stability test.

Supporting Tables

Table S1. The molar percent of Mn and Ru species for MnO_2/RuO_2 measured by ICP-OES analysis.

Sample	Test element	Sample Elemental Content W(%)	Atomic(%)
MnO_2/RuO_2	Mn	51.51%	85.27%
	Ru	16.37%	14.73%
	O	32.12%	/

Table S2. Percentage of O_{latt}, O_{vac} and O_{ads} in XPS of O 1s for MnO_2/RuO_2, MnO_2 and RuO_2.

Sample	O_{latt}	O_{vac}	O_{ads}
MnO_2/RuO_2	56.82%	34.66%	8.52%
MnO_2	70.42%	15.49%	14.09%
RuO_2	68.14%	23.72%	8.14%

Table S3. Comparison of the OER performance of MnO_2/RuO_2 in acid with some representative Ru-containing OER electrocatalysts.

Catalyst	Overpotential@ 10 mA·cm^{-2}(mV)	Tafel (mV·dec^{-1})	Stability	Ref.
MnO_2/RuO_2	**181**	**55.4**	**140h @ 10 mA·cm^{-2}**	**This work**
IrO_2-RuO_2@Ru	281	53.1	20h @ 1.5V	1
RuO_2 nanosheets	255	38.0	3h @ 10 mA·cm^{-2}	2
$Mn_{0.73}Ru_{0.27}O_{2-\delta}$	208	65.3	10h @ 10 mA·cm^{-2}	3
$RuIrO_2$	233	42.0	24h @ 1.45V	4
RuCu nanoalloy	270	75.8	20h @ 10 mA·cm^{-2}	5
$Y_{1.85}Zn_{0.15}Ru_2O_{7-\delta}$	290	36.9	10h @ 1.5V	6
Ru@Ir-O	238	91.3	40h @ 10 mA·cm^{-2}	7

$Ru_1Ir_1O_x$	204	71.3	100h @ 10 $mA \cdot cm^{-2}$	8
Ru@FLC	258	53.1	24h @ 1.49V	9
E-Ru/Fe NAs	238	44.8	9h @ 5 $mA \cdot cm^{-2}$	10
Ru-N-C	267	52.6	30h @ 10 $mA \cdot cm^{-2}$	11
IrRu@Te	220	35.0	20h @ 10 $mA \cdot cm^{-2}$	12
Si-RuO_x@C	220	53.0	100h @ 10 $mA \cdot cm^{-2}$	13
$RuO_2/(Co,Mn)_3O_4$	270	77.0	24h @ 10 $mA \cdot cm^{-2}$	14

Electrolyte is 0.5M H_2SO_4.

Table S4. ICP-OES results of dissolved Mn and Ru mass percent in the electrolyte of MnO_2/RuO_2 and RuO_2 after 1000 CVs tests.

Sample	Sample amount	Concentrations of Ru ion (μg mL^{-1})/Mn ion (μg mL^{-1})	Loss mass percent of Ru/Mn
MnO_2/RuO_2	1mg (0.16mg Ru)	0.027/0.333	0.85%/3.23%
RuO_2	1mg (0.76mg Ru)	0.42/0	2.75%/0

SI References

1. G. Li, S. Li, J. Ge, C. Liu and W. Xing, *J. Mater. Chem. A*, 2017, **5**, 17221-17229.
2. S. Laha, Y. Lee, F. Podjaski, D. Weber, V. Duppel, L. M. Schoop, F. Pielnhofer, C. Scheurer, K. Müller, U. Starke, K. Reuter and B. V. Lotsch, *Adv. Energy Mater.*, 2019, **9**, 1803795-1803802.
3. K. Wang, Y. Wang, B. Yang, Z. Li, X. Qin, Q. Zhang, L. Lei, M. Qiu, G. Wu and Y. Hou, *Energy Environ. Sci.*, 2022, **15**, 2356-2365.
4. Z. Zhuang, Y. Wang, C. Q. Xu, S. Liu, C. Chen, Q. Peng, Z. Zhuang, H. Xiao, Y. Pan, S. Lu, R. Yu, W. C. Cheong, X. Cao, K. Wu, K. Sun, Y. Wang, D. Wang, J. Li and Y. Li, *Nat. Commun.*, 2019, **10**, 4875-4884.
5. Y. Li, W. Zhou, X. Zhao, W. Cheng, H. Su, H. Zhang, M. Liu and Q. Liu, *ACS Appl. Energy Mater.*, 2019, **2**, 7483-7489.
6. Q. Feng, Q. Wang, Z. Zhang, Y. Xiong, H. Li, Y. Yao, X.-Z. Yuan, M. C. Williams, M. Gu, H. Chen, H. Li and H. Wang, *Appl. Catal. B*, 2019, **244**, 494-501.
7. J. Zhang, X. Fu, F. Xia, W. Zhang, D. Ma, Y. Zhou, H. Peng, J. Wu, X. Gong, D. Wang and Q. Yue, *Small*, 2022, **18**, 2108031-2108038.
8. J. He, X. Zhou, P. Xu and J. Sun, *Adv. Energy Mater.*, 2021, **11**, 2102883-2102891.
9. C. Shi, Y. Yuan, Q. Shen, X. Yang, B. Cao, B. Xu, B. Kang, Y. Sun and C. Li, *J. Colloid Interface Sci.*, 2022, **612**, 488-495.
10. Q. Yao, B. Huang, Y. Xu, L. Li, Q. Shao and X. Huang, *Nano Energy*, 2021, **84**, 105909-105916.
11. L. Cao, Q. Luo, J. Chen, L. Wang, Y. Lin, H. Wang, X. Liu, X. Shen, W. Zhang, W. Liu, Z. Qi, Z. Jiang, J. Yang and T. Yao, *Nat. Commun.*, 2019, **10**, 4849-4857.
12. J. Xu, Z. Lian, B. Wei, Y. Li, O. Bondarchuk, N. Zhang, Z. Yu, A. Araujo, I. Amorim, Z. Wang, B. Li and L. Liu, *ACS Catal.*, 2020, **10**, 3571-3579.
13. C. Liu, Y. Jiang, T. Wang, Q. Li and Y. Liu, *Adv. Sci.*, 2023, **10**, 2207429-2207435.
14. S. Niu, X.-P. Kong, S. Li, Y. Zhang, J. Wu, W. Zhao and P. Xu, *Appl. Catal. B*, 2021, **297**, 120442-120449.